Available online at www.sciencedirect.com
ScienceDirect
Ocean Engineering 34 (2007) 1882–1891
OCEAN ENGINEERING
www.elsevier.com/locate/oceaneng

# Three-dimensional wave patterns in long air cavities on a horizontal plane

Konstantin I. Matveev*

*School of Mechanical and Materials Engineering, Washington State University, Pullman, WA 99164-2920, USA*

Received 27 March 2006; accepted 9 August 2006
Available online 12 February 2007

**Abstract**

Significant drag reduction of large displacement vessels can be achieved by applying multi-wave air cavities arranged on the hull bottom. Waves generated on the air–water interface of air cavities impose requirements on the dimensions of a hull recess that accommodates the air cavity. An approximate model for calculating wave patterns in the critical upstream part of long air cavities in a simplified, horizontal-plane geometry is presented in this paper. The influence of the recess planform boundaries and other factors on the wave patterns is studied parametrically. Some hydrodynamic aspects of multi-wave air cavities are discussed.
© 2007 Elsevier Ltd. All rights reserved.

*Keywords:* Air cavity; Air lubrication; Drag reduction; Wave pattern

## 1. Introduction

The quest for higher speed and lower fuel consumption of marine transportation will always remain one of the main goals of naval architecture. A truly revolutionary and at the same time already validated (at least on some types of marine vehicles) technology is the lubrication of the wetted hull surface with an air layer (e.g., Latorre, 1997; Matveev, 2005). The air layer separates the ship hull from the water reducing hydrodynamic resistance. Drag reduction on well-designed air-lubricated surface ships (known as air-cavity ships or ACS) can typically be 15–30%, depending on the ship type.

The ACS concept implies a small disturbance to the water flow by an air layer and small power consumption for air injection to sustain the air cavity (about 2% of the total propulsive power). In this sense, the ACS concept is rather different from air-cushion vehicles, traditional surface-effect ships, and novel skirtless surface-effect ships (Tudem, 2002), which have large dimensions for the hull recess accommodating large air cushions/cavities and where a significant fraction of the total propulsive power is consumed by air injection.

The ACS technology has been already implemented on fast planing boats serially built in Russia (Matveev, 2005). Large displacement ACS prototype vessels were successfully tested 20–30 years ago (Butuzov et al., 1990), but the transition to the mass production of displacement ACS did not occur due to insufficient economic incentives at that time. With constantly growing demands for energy conservation, a huge market of displacement marine vessels may eventually adopt this concept. However, this will happen only if the feasibility of the ACS concept, or its derivative, for oceanic operations can be proven.

Two possible concepts for the air-cavity arrangement on displacement vessels are shown in Fig. 1. The first configuration (Fig. 1a) involves a set of wedges (cavitators) that initiate air cavities. This type could be retrofitted on existing conventional vessels. Several cavitators are needed along the ship bottom due to the instability of the long air cavities behind wedges.

A more advanced concept (Fig. 1b) utilizes a long recess on the ship bottom, accommodating a multi-wave air cavity. A set of wedges can still be used in this configuration, but they will be in contact with water only in some non-optimal operational modes. In the cruising

*Tel.: +1 360 490 3586.
*E-mail address:* matveev@hydrofoils.org.

0029-8018/$ - see front matter © 2007 Elsevier Ltd. All rights reserved.
doi:10.1016/j.oceaneng.2006.08.015

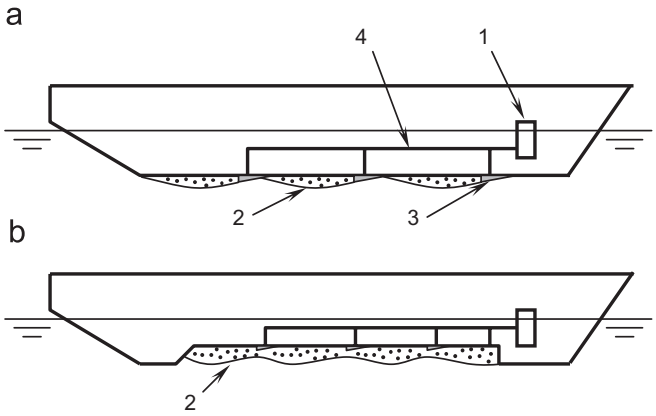


Fig. 1. Air-cavity systems applied on displacement vessels. 1: air blower, 2: air cavities, 3: cavitators, 4: gas pipeline. Air-cavity height and bottom recess height are shown not to scale.

regime, these cavitators would not touch the water flow. The hydrodynamic performance of this variant is higher, since frictional and form drag of cavitators of the first concept is eliminated. However, achieving a stable large air cavity without wetting the recess ceiling and with minimal air leakage, especially in sea waves, is a major research and development challenge.

The subject of this paper is the steady wave patterns in multi-wave air cavities that dictate the requirements for the air-cavity recess geometry, in particular, the height of the recess. The development of mathematical models for this class of flows was initiated by Butuzov (1966), who applied the theory of developed cavitating flows. Extensive results for fast air-cavity hulls in planing and semi-planing conditions were generated in two-dimensional and later in three-dimensional flows (e.g., Butuzov, 1981, 1988). Closely spaced two-dimensional air cavities on a horizontal plane were considered by Eller (1970) and Matveev (2003a). The effects of hydrodynamic singularities, imitating propulsors and ride control elements, were also studied in the same simplified configuration (Matveev, 2003b).

Gorbachev (1977a) considered a finite, multi-wave, rectangular cavity with a variable aspect ratio on a horizontal plane. A strong effect of the downstream end on the cavity characteristics was noticed, resulting in unphysical solutions with infinite wave amplitudes at some relations between the cavity length and the incident flow velocity. Little attention was paid to the three-dimensional structure of the wave patterns. However, it is known from experiments that three-dimensional flow phenomena play an important role in ACS performance. To our knowledge, no results were published on calculations of wave patterns in multi-wave air cavities on ship hulls, but apparently, a computer program has been developed at the Krylov Institute for the preliminary design of such systems (e.g., Sverchkov, 2002). There are some on-going efforts to develop potential-flow computational fluid dynamics (CFD) codes for modeling ship's air cavities (Choi et al., 2005; Thill et al., 2005).

This paper demonstrates a mathematical model for calculating wave patterns in the upstream part of a horizontal multi-wave air cavity and presents calculated wave patterns for systematic variation of relevant parameters, namely the cavity width, planform of the front step, parallel cavities, inclined gravity, trimmed step, and water surface tension. A general schematic of the problem is shown in Fig. 2.

The upstream part of a multi-wave cavity is the most critical place for the cavity performance. If the water surface reaches the recess ceiling in the upstream part of the cavity, then the effectiveness of air lubrication is reduced. If no wetting of the recess ceiling occurs in the upstream part of the cavity, then it is most likely that the air-cavity integrity will be maintained throughout the length of the cavity and the performance will be high.

In our theoretical model, the cavity is treated as infinite in the downstream direction, since the direct hydrodynamic influence of the downstream cavity end on the wave patterns near the front cavity step is minor for sufficiently long multi-wave air cavities. This is quite different from planing boats, where the influence of the closing geometry is critically important (Butuzov, 1981) and where the air cavities are considerably shorter than the unconstrained water surface wavelength. The air-cavity closure in multi-wave cavities remains important, but in a different way: it affects the air leakage from the cavity (and therefore, the air-cavity pressure) and the form drag of the hull part at the air-cavity reattachment. In our model, however, the air-cavity pressure is treated as an input parameter. We do not elaborate on the balance of air inside the cavity, and we address only the wave patterns at a given air-cavity pressure.

The horizontal surface outside the cavity planform boundaries is treated as an infinite wall. This greatly simplifies the analysis allowing us to linearize the problem. The linearization of boundary conditions on the air-cavity water surface implies small wave slopes. This is consistent

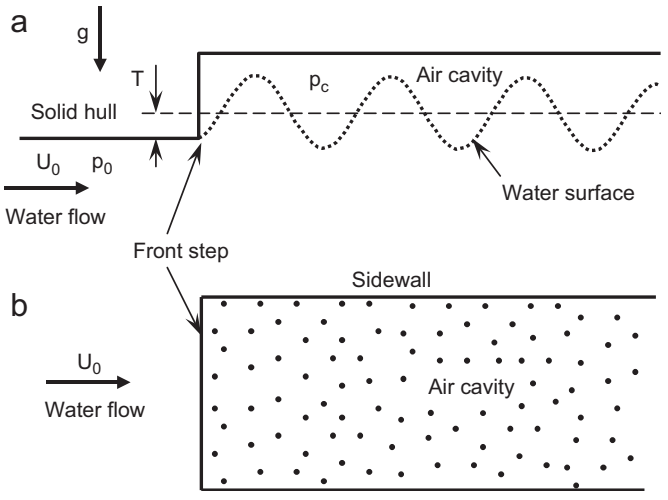


Fig. 2. General schematic of the problem. (a) Vertical-plane cross-sectional view. (b) Planform view.

with considering efficient air cavities that have small wave amplitudes.

The mathematical model in this paper uses the potential-flow linearized theory that has been applied for the air-cavity calculations (e.g., Butuzov, 1966, 1988; Aleksandrov, 1971; Gorbachev, 1977a; Matveev, 2003a, b). The novel aspects of this work include the consideration of a three-dimensional air cavity unclosed in the downstream direction, the emphasis on three-dimensional wave-pattern characteristics, and the systematic study of the effects of geometry and other external conditions.

In the air-cavity problems, the most commonly used dimensionless parameter is the cavitation number defined as follows:

$$\sigma = \frac{p_0 - p_c}{\rho U_0^2/2}, \tag{1}$$

where $p_0$ and $p_c$ are the pressure in the incident flow and inside the air cavity, respectively, $U_0$ is the ship speed, and $\rho$ is the water density. The cavitation number on ACS is small in magnitude. It is usually positive or close to zero on displacement-type vessels and negative on planing boats, which implies a small additional sinkage due to the air cavity on displacement ships and often a significant lift by the air cavity on planing boats.

The problem under consideration here is related to the flow behind transom-stern ships, which is another important subject in ship hydrodynamics (e.g., Schmidt, 1981; Maki et al., 2005). In fact, in the two-dimensional framework, the flows in the unclosed air cavity and behind the stern of a long ship are identical (Fig. 2a). The main dimensionless parameter in transom-stern flows is Froude number based on the transom static submersion $T$:

$$Fr_T = \frac{U_0}{\sqrt{gT}}, \tag{2}$$

where $g$ is the gravity acceleration. The transom-flow Froude number is related to the air-cavity cavitation number as $Fr_T^2 = 2/\sigma$. Three-dimensional or relatively short two-dimensional air cavities are significantly different from the transom-stern flows, since the free water surface behind the ship transom is usually unrestricted in the lateral and downstream directions.

## 2. Theoretical model and numerical approach

The water flow under a horizontal solid wall is considered (Fig. 3). A cavity recess is made in the wall to accommodate a macroscopic air cavity. The flow direction is parallel to the cavity side boundaries. The front boundary of the cavity (step) in the planform is not necessarily perpendicular to the incident flow velocity. If it is perpendicular, then the cavity is classified as rectangular. Flow is assumed irrotational, steady, and uniform upstream of the cavity. The liquid is incompressible and inviscid. The pressure inside the cavity is uniform and different from the static pressure in the incident liquid flow

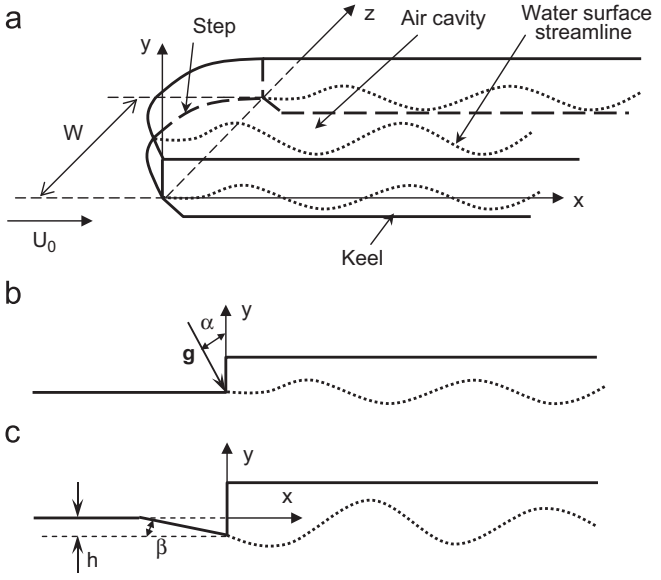


Fig. 3. (a) Schematic of the flow past an air cavity on horizontal wall. (b) Effective trim introduced by inclined gravity. (c) Locally trimmed step. $\alpha$, $\beta$, and $h$ are positive as depicted in (b) and (c).

at the wall level. Due to this pressure difference, the gravity-induced waves appear on the interface between the gas cavity and the flowing liquid. The motion of air in the cavity is neglected. The cavity is assumed to be infinitely long in the downstream direction. The water flow is sufficiently fast to achieve a separation at the front step. On the recess lateral boundaries, vertical keels in the longitudinal direction may be placed to contain the air inside the cavity. The goal of the analysis is to determine the wave-pattern characteristics on the air-cavity boundary in the upstream part of a cavity recess.

Under the imposed assumptions, the Bernoulli equation holds for the water flow at the cavity boundary:

$$p_0 + \frac{\rho U_0^2}{2} = p_c + \frac{\rho U_c^2}{2} + \rho g y_c - \rho g x \sin\alpha - \frac{\gamma}{R}, \tag{3}$$

where $p_0$ and $U_0$ are the pressure and velocity in the incident flow at the wall level, $\rho$ is the water density, $p_c$ is the uniform pressure inside the cavity, $U_c(x,z)$ is the water flow velocity at the cavity boundary with ordinate $y_c(x,z)$, $g$ is the gravitational constant, $\alpha$ is the inclination of the gravity field, $\gamma$ is the surface tension coefficient, and $R^{-1}$ is the local water surface curvature. A weakly non-uniform pressure and velocity field can be also approximated by adding disturbance terms in the Bernoulli equation (Ivanov, 1980; Matveev, 2003a), similar to the fourth term on the right-hand side of Eq. (3) that corresponds to the weakly inclined gravity field.

If we linearize the problem, assuming small wave slopes, as well as small deviation of the gravity vector from the $y$-axis, a linearized form of the Bernoulli equation can be

written as follows:

$$\frac{\sigma}{2}=\frac{u}{U_0}+\frac{2\pi y_c}{\lambda}-\frac{2\pi x\alpha}{\lambda}-\frac{\lambda}{We_\lambda}\left(\frac{\partial^2 y_c}{\partial x^2}+\frac{\partial^2 y_c}{\partial z^2}\right), \tag{4}$$

where $\sigma=(p_0-p_c)/(\rho U_0^2/2)$ is the cavitation number, $u(x,z)$ is the velocity perturbation along the $x$-axis, $\lambda=2\pi U_0^2/g$ is the wavelength on unconstrained free water surface, and $We_\lambda=\rho U_0^2\lambda/\gamma$ is the Weber number based on the free-surface wavelength.

The accurate accounting for the sidewalls would considerably complicate mathematical modeling. However, it was established that the influence of sidewalls on the air-cavity surface is significant only in their vicinities, and the sidewall presence can be neglected in approximate analyses (Aleksandrov, 1971; Gorbachev, 1977a; Butuzov, 1988). The only effect of these walls in our modeling is to contain the air cavity on lateral sides. Nevertheless, it should be kept in mind that calculated wave patterns (presented in the next section) are not accurate in the regions close to the sidewalls.

We will solve Eq. (4) by a method of hydrodynamic singularities, introducing sources in the horizontal plane $y=0$ of the air cavity. The staggered arrangement is applied for the collocation points, where Eq. (4) is fulfilled (Fig. 4), and for the sources. This scheme eliminates reflection of the waves from the downstream boundary of a numerical domain (e.g., Bertram, 2000; Semenenko, 2003) and effectively simulates the upstream part of an unclosed or sufficiently long air cavity.

From the linearized kinematic condition on the water surface, the source intensity can be approximately related to a derivative of the water surface elevation in the main flow direction:

$$\frac{q_{i-1}+q_i}{2\Delta x\Delta z}=-2U_0\frac{\partial y_c}{\partial x}(x_i,z_i), \tag{5}$$

where $(x_i,z_i)$ are the coordinates of a collocation point under consideration, $q_{i-1}$ and $q_i$ are the intensities of its neighboring upstream and downstream sources, and $\Delta x$ and $\Delta z$ are the distances between the source positions in $x$- and $z$-directions. The $x$-component of the velocity perturbation at a collocation point is the sum of velocities

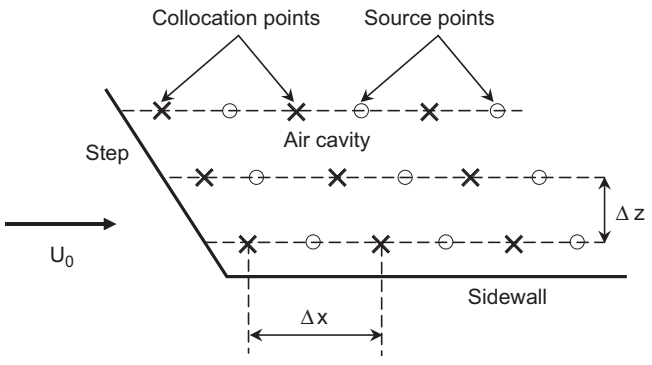


Fig. 4. Planform view on disposition of collocation points and sources inside air cavity.

induced by the distribution of sources:

$$u(x_i,z_i)=\frac{1}{4\pi}\sum_j\frac{q_j}{r_{i,j}^2}\frac{x_i-x_j^s}{r_{i,j}}, \tag{6}$$

where $r_{i,j}=\sqrt{(x_i-x_j^s)^2+(z_i-z_j^s)^2}$ is the distance between a collocation point with index $i$ and a location of the source with index $j$. The water surface elevation on the air-cavity boundary can be recovered by $x$-integration of the source intensities using Eq. (5) and the boundary conditions at the step that assume smooth flow separation in the $x$-direction:

$$y_c|_{step}=-h,\quad \left.\frac{\partial y_c}{\partial x}\right|_{step}=-\beta, \tag{7}$$

where $h$ and $\beta$ are the characteristics of the longitudinal cross-section of the step, as shown in Fig. 3c; $\beta$ is small. For non-zero $h$ and $\beta$, there is an additional contribution to the velocity perturbation due to a trimmed step, which can also be modeled by distributed hydrodynamic sources. For a rectangular cavity and a uniform step, this velocity perturbation is given by the formula

$$u_1(x_i,z_i)=\frac{U_0\beta}{2\pi}\ln\left|\frac{[(z_i-W)+\sqrt{(x_i+h/\beta)^2+(z_i-W)^2}][z_i+\sqrt{x_i^2+z_i^2}]}{[(z_i-W)+\sqrt{x_i^2+(z_i-W)^2}][z_i+\sqrt{(x_i+h/\beta)^2+z_i^2}]}\right|. \tag{8}$$

This velocity is added to $u(x,z)$ from Eq. (6) before substituting into Eq. (4).

Thus, the surface ordinate and velocity perturbation in Eq. (4) can be represented through the source distribution, and the resulting system of linear equations can be solved numerically for source intensities. Afterwards, the water surface elevations can be found.

As was noted in the Introduction, the air-cavity and ship-transom flows are equivalent in the case of a two-dimensional flow. In Fig. 5, our numerical solution (for zero surface tension, right-angle step, and vertical gravity) is compared with the asymptotic solution of Schmidt (1981) for water surface ordinates in the transom flow, valid at sufficiently large distances behind the right-angle transom:

$$\frac{y}{\lambda\sigma}=\frac{1}{4\pi}\left[1-\sqrt{2}\cos\left(\frac{2\pi}{\lambda}x+\frac{\pi}{8}\right)\right], \tag{9}$$

with $(x,y)=(0,0)$ being the transom point location and the $x$-axis is directed downstream. In the two-dimensional reduction of our numerical model, we found that discretization density of 30 sources per a wavelength has produced numerical results with sufficient convergence. As seen in Fig. 5, numerical results and those of Eq. (9) are in satisfactory agreement except for the very vicinity of the transom, where Eq. (9) is invalid, and for the region near the downstream boundary, where the end of the domain deteriorates the accuracy of a numerical solution.

For three-dimensional problems presented in the next section, the discretization interval $\Delta x$ was chosen as at least

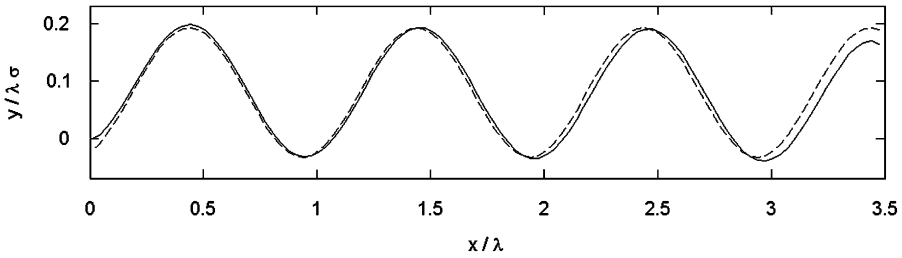


Fig. 5. Solid curve: numerically found two-dimensional water surface profile behind the step. Dashed curve: analytical asymptotic solution (Schmidt, 1981).

$\frac{1}{30}$th of the free wavelength and $\Delta z$ was chosen as either $\Delta x$ or $\frac{1}{30}$th of the cavity width, whichever less. The length of the numerical domain in the flow direction was at least $3.5\lambda$, and results are presented for the upstream region of length $3\lambda$, where the influence from the downstream boundary of the numerical domain is minimal.

## 3. Results and discussion

We calculated wave patterns for a series of air-cavity configurations and conditions. These include a rectangular cavity with different widths $W$ (Fig. 6a), a cavity with a parabolic step of different elongations $H$ (Fig. 6b), a cavity with an oblique step (Fig. 6c), and a system of two parallel cavities with different spacing $S$ (Fig. 6d). In these configurations, the gravity vector is assumed vertical, the step longitudinal cross-section is at a right angle to the incident flow, and the surface tension is ignored. Additionally, the effects of an inclined gravitational field (Fig. 3b), a trimmed step (Fig. 3c), and a surface tension (finite $We$) were considered separately and only for rectangular cavities with $W/\lambda = 1$.

The wave patterns computed for rectangular air cavities of different widths (with respect to the unconstrained water wavelength) are shown in Fig. 7. For a fixed cavity width, lower $W/\lambda$ ratio implies higher ship speed. The water surface elevation is given in Fig. 7a–d as finely graded surface plots: white color is assigned to the highest elevation (wave crest), while regions with the lowest ordinates (wave trough) are black.

The wave patterns in the air cavity consist of transverse waves originating from the step and divergent wave systems formed at the sidewalls. At a sufficiently large $W/\lambda$ ratio, the water surface in the upstream part of the cavity and outside the divergent wave systems (i.e., near the cavity centerline) is similar to the two-dimensional flow. At a sufficiently low $W/\lambda$ ratio, divergent waves greatly influence even the first transverse wave, including its centerline region. The wavelength of the transverse wave system becomes shorter with decreasing $W/\lambda$ ratio, similar to numerical findings of Gorbachev (1977a). The three-dimensional character of the air-cavity waves noticeable in Fig. 7 is also apparent in experiments.

Interactions between wave systems result in local amplification of the wave amplitudes, which may require

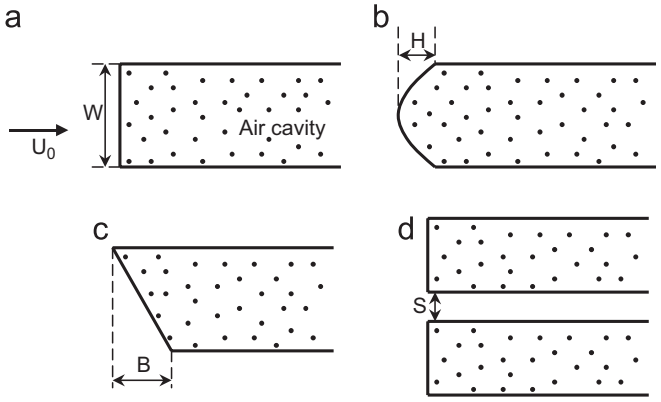


Fig. 6. Some studied schematics. (a) Rectangular air cavity with different width/wavelength ratio. (b) Parabolic step. (c) Asymmetric cavity with oblique step. (d) Parallel cavities.

large vertical dimensions of the cavity recess (in order to maintain air-cavity integrity) and longitudinal keels (to minimize lateral air leakage). Under some conditions, the flow formations similar to "rooster tails" behind transom-stern hulls may be generated in the air cavity. Special attention should be paid to the water surface extremes in the upstream part of the cavity, since the downstream waves are more significantly affected by viscous and nonlinear effects. The local, specially designed increase in the recess height above the water surface maxima may help in preventing wetting of the ceiling at the designed operational condition. However, this advantage is likely to disappear at other ship speeds and loadings and in rough seas, unless the ceiling geometry is dynamically adapted. Such hull modifications would also lead to structural issues and higher construction costs.

The influence of an elongated parabolic step, often seen in modern air-cavity arrangements to maximize the air-cavity area (e.g., Sverchkov, 2002), is shown in Fig. 8 for one relative width $W/\lambda = 1$. The reduced transverse wave amplitudes at the centerline in the upstream part of the cavity (at least in the first two transverse waves) are apparent when a parabolic step is introduced. This is an important advantage of the cavity with a curved front step. Some calculated wave patterns manifest maximum amplitudes in the divergent waves close to sidewalls and in the interference centerline regions a few wavelengths downstream of the step. However, amplitudes in the wave

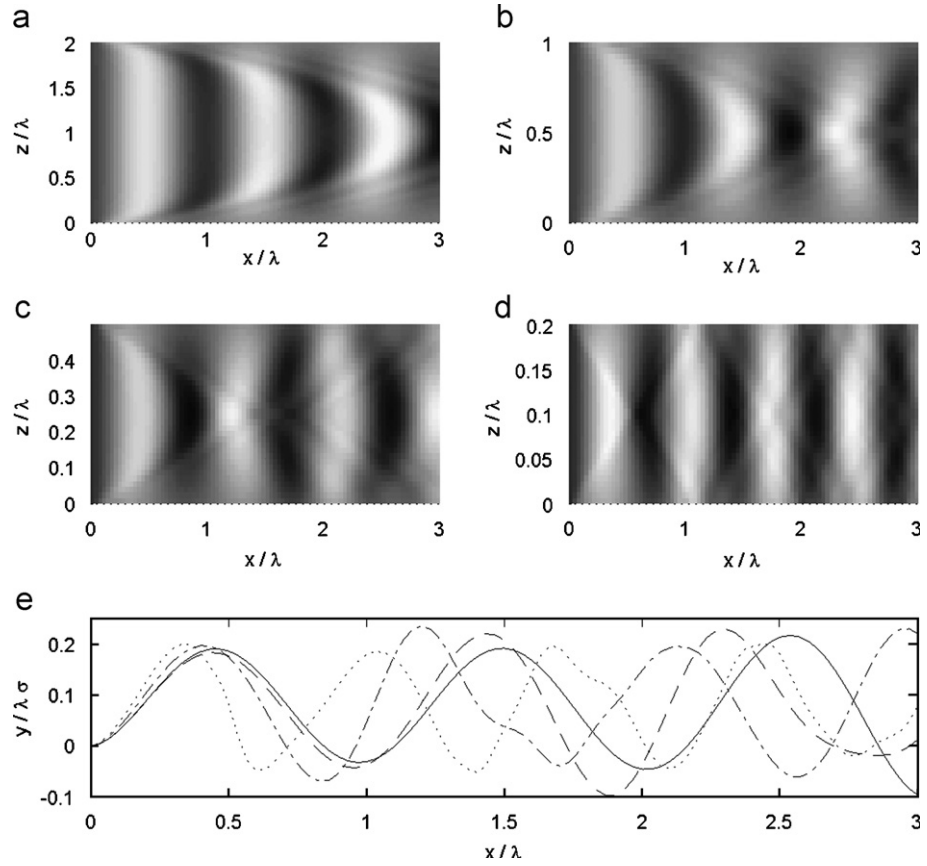


Fig. 7. (a)–(d) Wave patterns in the rectangular air cavity. (e) Wave profiles on the cavity centerline for different cavity width/wavelength ratio. The flow direction is from left to right. (a) $W/\lambda = 2$; corresponding centerline wave profile is shown by solid curve in (e). (b) $W/\lambda = 1$; dashed curve. (c) $W/\lambda = 0.5$; dash-dotted curve. (d) $W/\lambda = 0.2$; dotted curve.

systems with shorter wavelengths are likely to be smaller in reality due to viscous, nonlinear, and sidewall effects. Moreover, in some configurations of cargo ship models with near-parabolic steps, the longitudinal side keels are not even needed for achieving large stable cavities and high hydrodynamic performance.

Air cavities with oblique (in horizontal plane) steps can be utilized close to the lateral sides of large-beam monohulls and on asymmetric catamarans. The influence of the obliqueness angle is illustrated in Fig. 9. Extreme water surface ordinates are displaced to the cavity side that is shifted downstream.

The effect of two cavities placed in parallel (as in Fig. 6d) is presented in Fig. 10. Even at spacing $S/W = 0.1$ (for $W/\lambda = 1$), the influence of a neighboring cavity is weak (Fig. 10a), and the wave pattern in this cavity is not that different from that in Fig. 7b. At a smaller spacing, the wave pattern approaches that of a single cavity with doubled width, so this wave structure (Fig. 10b) becomes similar to that on the portside half of the cavity in Fig. 7a.

An important operational factor influencing the air-cavity wave pattern and the effectiveness of the air-cavity drag reduction is the ship's trim. The influence of a trim angle (or the inclination of the gravity field in our mathematical model as shown in Fig. 3b) is demonstrated in Fig. 11. The bow-up trim condition displaces the water surface above the ship's base plane, requiring larger recess height to keep the air-cavity integrity. The bow-down trim produces the opposite effect on the air-cavity boundary, thus reducing demand for the recess height, but possibly requiring an increase of keels for minimizing lateral air leakage. On real ships, however, additional factors (e.g., non-uniform velocity and pressure distribution over the hull) also significantly affect water surface elevations in the cavity. It is likely that the optimal operational trim for most displacement air-cavity vessels is near zero, such as was found in the tests of a supertanker model (Gorbachev, 1977b). This generally corresponds to a certain non-zero trim at stop.

The wave pattern inside the air cavity is also affected by the ship hull surface outside the cavity. One of the most effective and simplest means for optimizing the air cavity is to adjust a relatively small ship hull area at the front of the air cavity (Fig. 3c). The effect of such modification is shown in Fig. 12. While forcing the flow downward leads to higher wave amplitudes, the upwardly trimmed step results in significantly lower water surface amplitudes. This method is expected to be of great value in practical applications, and can even assist in maintaining the air cavity under various operational conditions. More

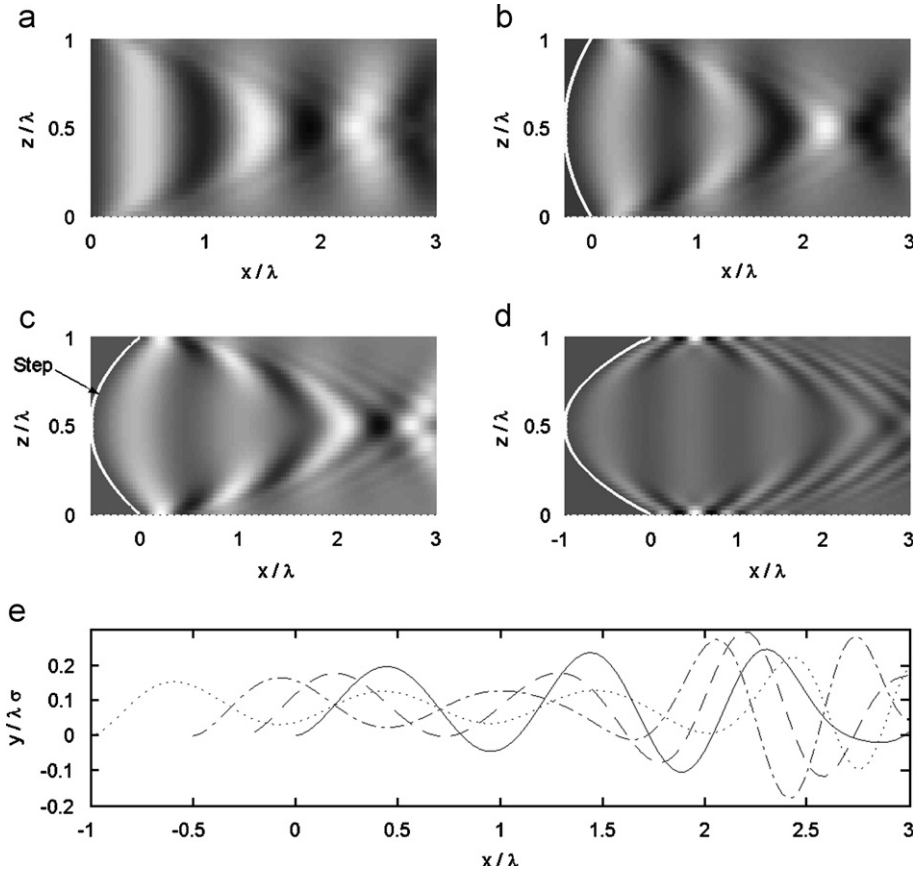


Fig. 8. (a)–(d) Wave patterns in the air cavity with $W/\lambda = 1$. (e) Wave profiles on the cavity centerline for different elongations of a parabolic step. (a) $H/\lambda = 0$; corresponding centerline wave profile is shown by solid curve in (e). (b) $H/\lambda = 0.25$; dashed curve. (c) $H/\lambda = 0.5$; dash-dotted curve. (d) $H/\lambda = 1$; dotted curve.

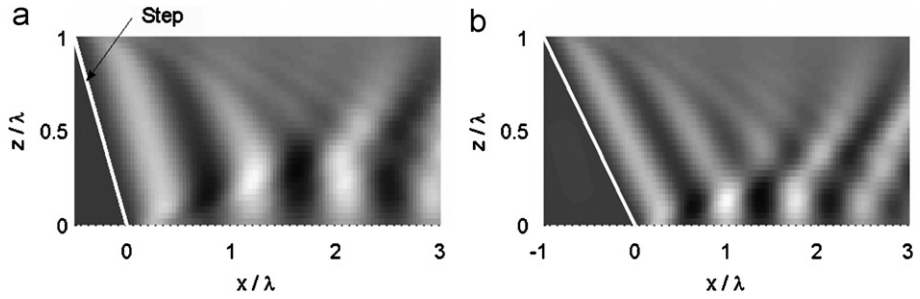


Fig. 9. Wave patterns in the asymmetric air cavity with $W/\lambda = 1$ and different inclinations of an oblique step. (a) $B/\lambda = 0.5$. (b) $B/\lambda = 1$.

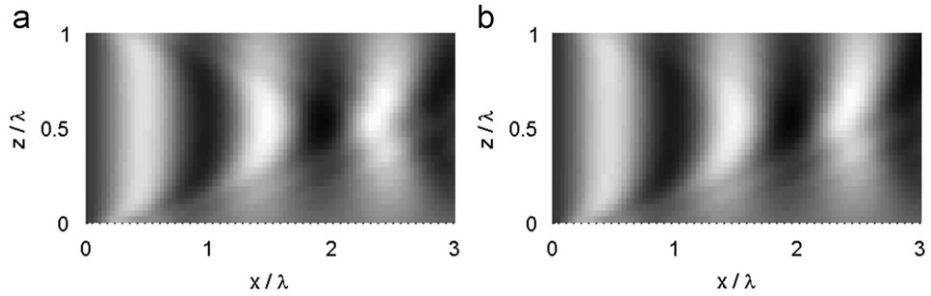


Fig. 10. Wave patterns in the portside cavity in the system of two parallel rectangular cavities with $W/\lambda = 1$. (a) $S/\lambda = 0.1$. (b) $S/\lambda = 0.05$.

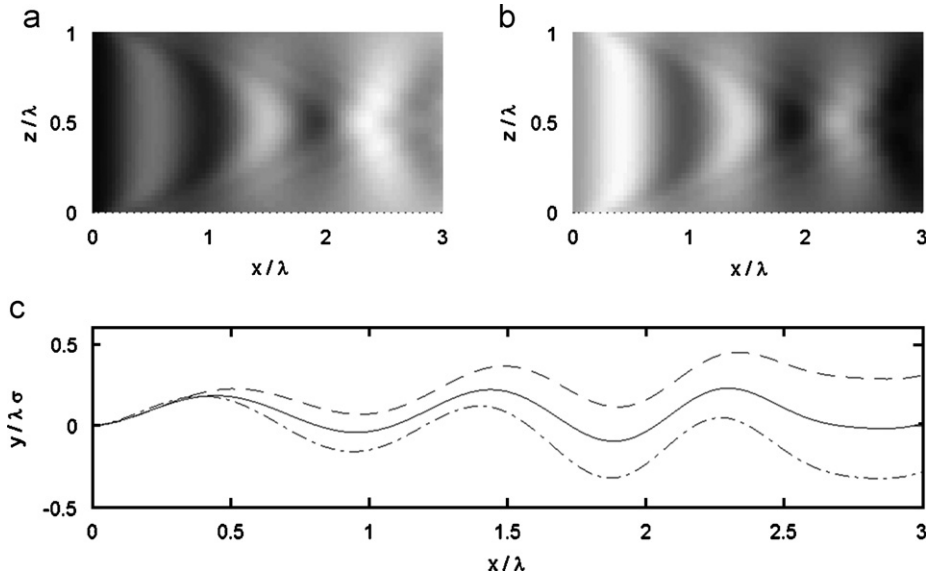


Fig. 11. (a), (b) Wave patterns in the rectangular air cavity with $W/\lambda = 1$. (c) Wave profiles on the cavity centerline for different gravity inclinations. (a) $\alpha/\sigma = 0.1$ ($\sigma$ is positive); corresponding centerline wave profile is shown by dashed curve in (c). (b) $\alpha/\sigma = -0.1$; dash-dotted curve. Solid curve in (c) corresponds to $\alpha = 0$.

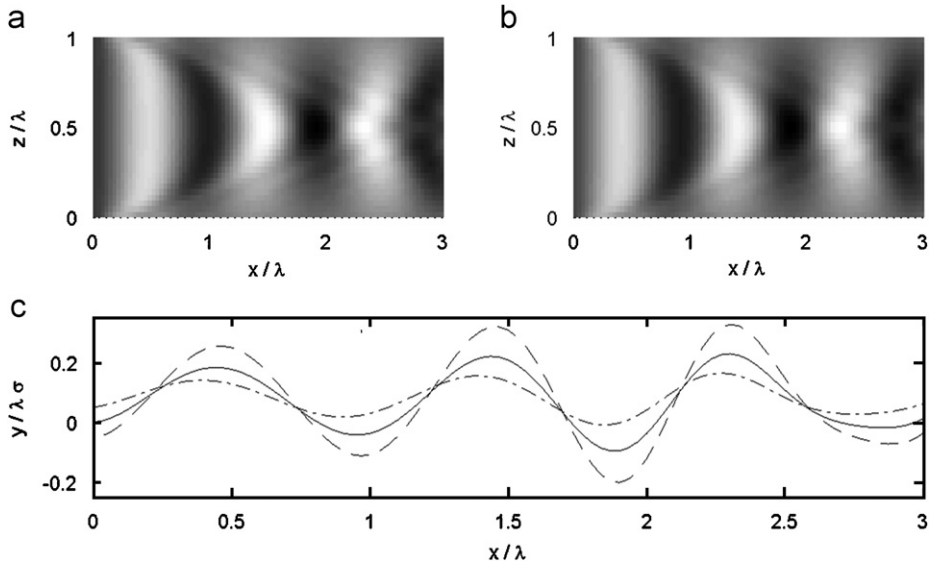


Fig. 12. (a), (b) Wave patterns in the rectangular air cavity with $W/\lambda = 1$. (c) Wave profiles on the cavity centerline for different step trimming. (a) $\beta/\sigma = 0.1$ and $h/(\lambda\sigma) = 0.05$ ($\sigma$ is positive); corresponding centerline wave profile is shown by dashed curve in (c). (b) $\beta/\sigma = -0.1$ and $h/(\lambda\sigma) = -0.05$; dash-dotted curve. Solid curve in (c) corresponds to $\beta = h = 0$.

sophisticated geometries of the step in both transverse and longitudinal directions can be sought. A related problem for minimizing wake wash behind a two-dimensional transom ship by selecting an appropriate stern geometry was considered by Schmidt (1981).

In testing low-speed small-scale ACS models, the water surface tension can play a role. The effect of low Weber numbers on the wave pattern in the rectangular cavity with $W/\lambda = 1$ is illustrated in Fig. 13. With increasing influence of surface tension, the centerline wave profile manifests shorter and higher waves. However, a noticeable influence of surface tension on the wave pattern occurs only at low speeds. From model testing experience (Sverchkov 2002), it is known that the influence of surface tension on the measured resistance of standard-size low-speed displacement ACS models can be completely neglected for $We_\lambda > 18,000$.

## 4. Concluding remarks

A simplified three-dimensional mathematical model based on a linearized potential-flow theory and parametric

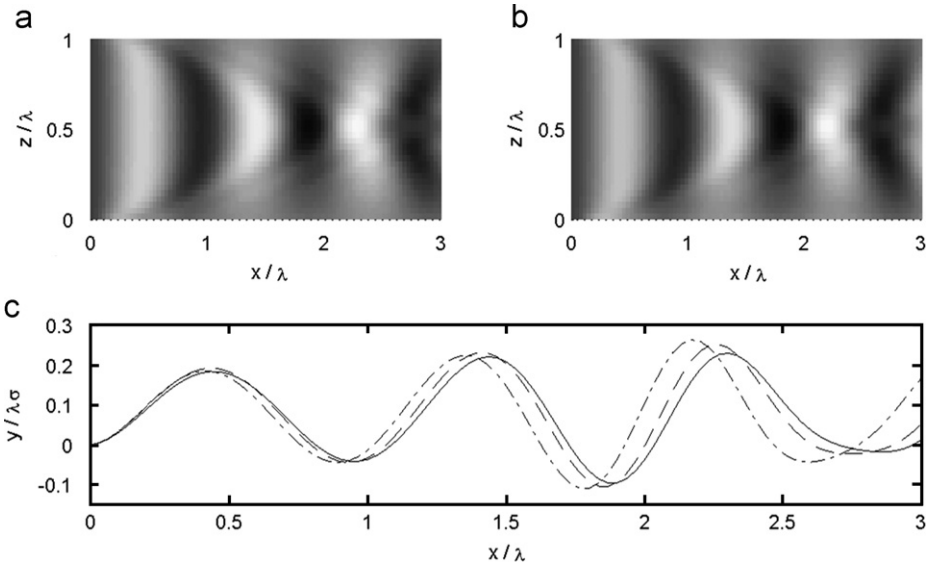


Fig. 13. (a), (b) Wave patterns in the rectangular air cavity with $W/\lambda = 1$. (c) Wave profiles on the cavity centerline for different Weber number ($\sigma$ is positive). (a) $We_\lambda = 6000$; corresponding centerline wave profile is shown by dashed curve in (c). (b) $We_\lambda = 2000$; dash-dotted curve. Solid curve in (c) corresponds to $We_\lambda = \infty$.

results for the wave patterns inside the multi-wave air cavities on a horizontal plane are presented in this paper. A transverse wave system is found originating at the front step with divergent waves generated at the sidewalls. The interference between wave systems leads to the appearance of local extremes of the water surface ordinates that must be accounted for in selecting heights of the air-cavity recess and longitudinal keels. The geometrical features of the air-cavity boundaries, as well as external conditions, significantly affect the wave patterns inside air cavities.

Experimental studies are needed for validating this model and for establishing its limitations. Perhaps, empirical corrections can be introduced for practical application of this theory, similar to the viscous damping in the extended thin-ship theory (e.g., Tuck et al., 2002). Little information for measured wave patterns in air cavities is currently available in open literature, and corresponding conditions are described insufficiently for making comparisons. Due to the smallness of some characteristic dimensions involved (e.g., height of the wetted area on sidewalls), it is expected that a scale effect may play an important role in conducting model tests and extrapolating model results to the full scale.

Applications of modern CFD methods with inclusion of viscosity, air flow, and cavity reattachment should greatly benefit the ACS technology. Again, validation of CFD methods for the water and air flows specifically around ACS hulls will be necessary prior to applying these tools in design practice.

## Acknowledgment

The author thanks Ralph Duncan for help in preparing this paper.

## References

Aleksandrov, K.A., 1971. Results of the study of cavitating flows behind a finite-aspect wedge on the infinite plate. Transactions of NTO Sudprom 168, 140–154 (in Russian).

Bertram, V., 2000. Practical Ship Hydrodynamics. Butterworth-Heinemann, Oxford.

Butuzov, A.A., 1966. Limiting parameters of an artificial cavity formed on the lower surface of a horizontal wall. Fluid Dynamics 1 (2), 167–170.

Butuzov, A.A., 1981. Application of artificial cavitation for reducing hydrodynamic drag of a planing hull. Shipbuilding Questions, Ship Design Series 28, 3–20 (in Russian).

Butuzov, A.A., 1988. Spatial linearized problems on flow around ship bottom with artificial cavitation. Shipbuilding Questions, Ship Design Series 8, 1–18 (in Russian).

Butuzov, A.A., Gorbachev, Y.N., Ivanov, A.N., Kalyuzhny, V.G., Pavlenko, A.N., 1990. Reduction of ship resistance using ventilated gas cavities. Shipbuilding 11, 3–6 (in Russian).

Choi, J.-K., Hsiao, C.-T., Chahine, G.L., 2005. Design trade-off analysis for high performance ship hull with air plenums. In: Proceedings of the Second International Symposium on Seawater Drag Reduction, Busan, Korea.

Eller, A.O., 1970. Determination of the parameters of the infinite air cavity system located on the lower side of the unbounded horizontal wall. Transactions of Krylov SRI 258, 54–62 (in Russian).

Gorbachev, Y.N., 1977a. Study of the influence of the step aspect ratio on the parameters of cavities with wave profiles. Shipbuilding Questions, Ship Design Series 12, 57–64 (in Russian).

Gorbachev, Y.N., 1977b. Experimental studies of a supertanker model with the bottom air cavity. Shipbuilding Questions, Ship Design Series 12, 79–86 (in Russian).

Ivanov, A.N., 1980. Hydrodynamics of Developed Cavitating Flows. Sudostroenie, Leningrad, 177–181 (in Russian).

Latorre, R., 1997. Ship hull drag reduction using bottom air injection. Ocean Engineering 24, 161–175.

Maki, K., Doctors, L.J., Beck, R.F., Troesch, A.W., 2005. Transom-stern flow for high-speed craft. In: Proceedings of the Fifth International Conference on Fast Sea Transportation, St. Petersburg, Russia.

Matveev, K.I., 2003a. Two-dimensional modeling of the limiting air cavity system. In: Proceedings of the 41st Aerospace Sciences Meeting and Exhibit, Reno, NV, USA. AIAA Paper No. 2003-0624.

Matveev, K.I., 2003b. On the limiting parameters of artificial cavitation. Ocean Engineering 30, 1179–1190.

Matveev, K.I., 2005. Application of artificial cavitation for reducing ship drag. Oceanic Engineering International 9 (1), 35–41.

Schmidt, G.H., 1981. Linearized stern flow of a two-dimensional shallow-draft ship. Journal of Ship Research 25 (4), 236–242.

Semenenko, V.N., 2003. Calculation of two-dimensional unsteady super-cavitating flows around wedges and hydrofoils. Oceanic Engineering International 6 (2), 66–73.

Sverchkov, A.V., 2002. Perspectives of artificial cavity application aimed at resistance reduction of ocean/river ships. In: Proceedings of the Third International Shipbuilding Conference, St. Petersburg, Russia.

Thill, C., Toxopeus, S., van Walree, F., 2005. Project energy-saving air-lubricated ships (PELS). In: Proceedings of the Second International Symposium on Seawater Drag Reduction, Busan, Korea.

Tuck, E.O., Scullen, D.C., Lazauskas, L., 2002. Wave patterns and minimum wave resistance for high-speed vessels. In: Proceedings of the 24th Symposium on Naval Hydrodynamics, Fukuoka, Japan.

Tudem, U.S., 2002. The challenge of introducing innovative air lifted vessels to the commercial market. In: Proceedings of the 18th Fast Ferry Conference, Nice, France.